

# The mARM3D spatially distributed soil evolution model: Three-dimensional model framework and analysis of hillslope and landform responses

Sagy Cohen,<sup>1,2</sup> Garry Willgoose,<sup>1</sup> and Greg Hancock<sup>2</sup>

Received 20 September 2009; revised 23 May 2010; accepted 14 June 2010; published 20 October 2010.

[1] We present a three-dimensional landscape-pedogenesis model, mARM3D (matrices ARMOUR 3D), which simulates soil evolution as a function of erosion and pedogenic processes. The model simulates the discretized soil profile for points on a spatial grid. The approach, using transition matrices, is computationally efficient and allows the simulation of large-scale spatial coupling and long-term soil evolution. We study the effect of the depth-dependent soil-weathering rate (i.e., the rate of soil particle breakdown) and bedrock-lowering rate (i.e., the rate of conversion of bedrock to soil). The difference in depth-dependent weathering functions has a significant effect on the in-profile soil properties through depth, specifically particle size grading. However, the depth dependency has a relatively minor effect on the surface properties of the soil profile, with all weathering functions generating very similar surface properties. The surface properties were a function of the cumulative amount of weathering (i.e., the integral of the weathering function over exhumation) with finer surface grading for higher weathering rates. Soil thickness could be estimated without explicitly modeling soil thickness. Thickness was negatively correlated with surface median grain size. As thickness decreases, the surface grading coarsens. This was driven by surface erosion, where as surface grading coarsens, erosion decreases and the soil deepens. Weathering and erosion interact to spatially organize the surface soil grading with a log-log relationship between surface grading, contributing area, and local slope. This relationship was independent of the weathering function. This relationship might be useful for the spatial description of soil properties in digital soil mapping.

**Citation:** Cohen, S., G. Willgoose, and G. Hancock (2010), The mARM3D spatially distributed soil evolution model: Three-dimensional model framework and analysis of hillslope and landform responses, *J. Geophys. Res.*, 115, F04013, doi:10.1029/2009JF001536.

## 1. Introduction

[2] Many hydrological and geomorphological processes have strong links to soil properties. For example, soil erosion and runoff vary in response to changes in soil texture. However, many large-scale hydrological and geomorphological models do not account for varying soil properties. This is for two main reasons: (1) The spatial distribution of these properties is unknown at the scale of modeling, and (2) the relationships for soil functional characteristics (e.g., hydrologic conductivity) used in the model are uncertain. Therefore models tend to assume soil homogeneity over their modeled domain despite the significance of soil grading and/or texture to the process description.

[3] Soil properties vary in space and time as soil evolves in response to sediment transport and weathering processes. It may reach a state of dynamic equilibrium in which the rate of soil production is in equilibrium with soil removal and tectonics. However, when simulating long-term processes (e.g., landform evolution) or time-varying conditions (e.g., climate change) the dynamics of the changes in soil properties may impact on the simulated processes [Minasny and McBratney, 2006].

[4] In this context describing soil spatiotemporal variability can best be achieved by a physically based landscape-pedogenesis model. The importance of soil evolution modeling, for geomorphology and soil studies, has been well documented in the literature [e.g., Minasny and McBratney, 1999]. The soil science community has been developing pedogenesis models for many years [e.g., Jenny, 1941]. Two recent reviews examined pedogenesis modeling. Samouëlian and Cornu [2008] focused on soil process description in models. They viewed existing models as limited in both their dimensionality (i.e., limited in their ability to model both spatial and/or temporal dynamics simultaneously) and the

<sup>1</sup>School of Engineering, University of Newcastle, Callaghan, New South Wales, Australia.

<sup>2</sup>School of Environmental and Life Sciences, University of Newcastle, Callaghan, New South Wales, Australia.

pedogenic processes they modeled, describing only the solid phase of soil development (i.e., material sediment transport but not dissolution). They argued that a more detailed description of pedogenesis is required which will need to include the soil water cycle and its effect on the processes. However, they predict that for such a modeling framework "... early versions will likely be monstrous in computing requirements ..." [Samouëlian and Cornu, 2008, p. 408].

[5] On the other hand, *Minasny et al.* [2008] focused on regional-scale simulations of soil properties. They argued that a mass balance mechanistic model is likely the best approach and that the main challenge today is linking landscape-scale models [e.g., *Minasny and McBratney*, 2006] and soil-profile-scale models [e.g., *Legros and Pedro*, 1985; *Salvador-Blanes et al.*, 2007]. *Yoo and Mudd* [2008a] presented a physically based model which combined a mass balance of geochemical soil processes and lateral sediment flux equations. Their model only allowed a coarse discretization spatially and within the profile (three layers: bedrock, saprolite and colluvium). This coarse discretization was, in part, due to computational constraints.

[6] In this paper the matrices ARMOUR 3d (mARM3D) model is presented. It simulates long-term and large-scale (100,000s years over 1000s pixels) soil-profile evolution on the basis of a novel numerical approximation that results in a highly modular and computationally efficient platform. mARM3D was built on the foundations of mARM1D [Cohen et al., 2009] by adding the capability to model pedogenesis using a high-resolution discretization of the soil profile. The mARM3D model is a significant advance in landscape-pedogenesis modeling as it explicitly models soil grading evolution (in tens of grading size classes) and its spatial distribution (with 10s of profile layers for tens of thousands of pixels across the landscape).

[7] The model capabilities are described here in a series of hillslope- and landscape-scale simulations. The mARM3D configuration is kept simple in this paper by modeling only surface armoring (selective erosion) and physical weathering. This was done to simplify the interpretation of results and is not a limitation of the modeling approach. These simulations are used to examine the effect of weathering depth dependency on soil evolution and resulting distribution. While the model is designed for inclusion in a landform evolution model this paper only uses fixed elevation landforms. Again this was done to simplify the interpretation of the results in this paper.

## 2. The mARM3D Model

[8] As noted above mARM3D is based on the mARM1D model [Cohen et al., 2009]. mARM1D models the evolution of soil grading as a function of armoring and weathering in a single layer at the soil surface for a one-dimensional hillslope. It uses a state-space matrix model to calculate changes in soil grading over a time step,

$$\begin{bmatrix} g_1 \\ g_2 \\ \vdots \\ g_k \end{bmatrix}_{t+1} = \begin{bmatrix} g_1 \\ g_2 \\ \vdots \\ g_k \end{bmatrix}_t + \begin{bmatrix} A_{11} & A_{12} & \cdots & A_{1k} \\ A_{21} & A_{22} & \cdots & A_{2k} \\ \vdots & \vdots & \ddots & \vdots \\ A_{k1} & A_{k2} & \cdots & A_{kk} \end{bmatrix} \cdot \begin{bmatrix} g_1 \\ g_2 \\ \vdots \\ g_k \end{bmatrix}_t, \quad (1)$$

or in a more conceptually convenient matrix-vector notation,

$$\underline{g}_{t+1} = (\mathbf{I} + \mathbf{A}) \cdot \underline{g}_t, \quad (2)$$

where  $\underline{g}_t$  is a vector for the particle size grading distribution of the soil at time  $t$  and the  $k \times k$  matrix  $\mathbf{A}$  defines how the grading changes for a single layer in a single time step from  $t$  to  $t + 1$ . The grading distribution is represented by  $k$  size classes where in the discussion below 1 is the smallest size grading fraction and  $k$  is the largest. As discussed by *Cohen et al.* [2009], it is sometimes convenient to express  $\underline{g}$  as the proportion (or percentage) of the grading by mass in that class, while at other times it is more convenient to express it as the absolute mass in the class in that layer per unit plan area. In this paper the latter definition is used. The details of how the individual elements of the matrix  $\mathbf{A}$  are populated are discussed briefly below. More detail can be found in the work of *Cohen et al.* [2009].

[9] Equations (1) and (2) describe how a single layer of soil changes. The extension to modeling the entire depth of a soil profile in mARM3D is relatively straightforward. Figure 1 shows that the soil profile is modeled with a number of layers. The top layer is the surface layer exposed directly to surface processes like erosion. It is underlain by  $n$  layers of soil. These layers can be of different thicknesses, but for simplicity they are all the same thickness in this paper. The layer thickness is temporally constant. Underlying these  $n$  soil layers is a semi-infinite soil layer, which is considered an infinite source of bedrock to layer  $n$  (directly above it). Vertical gradients are not modeled within a layer unit so each layer is perfectly mixed. The coordinate system is relative to the soil surface. This definition of coordinates means that when erosion occurs the layer boundaries are moved down with a velocity equal to the erosion rate (in units of depth/unit time) through the soil with the soil particles stationary. Thus when erosion occurs material from the layer below has to be supplied to the layer above to maintain the layer thickness.

[10] Mathematically this can be written in matrix form as

$$\begin{bmatrix} \underline{g}_s \\ \underline{g}_1 \\ \vdots \\ \underline{g}_n \\ \underline{g}_\infty \end{bmatrix}_{t+1} = \begin{bmatrix} \underline{g}_s \\ \underline{g}_1 \\ \vdots \\ \underline{g}_n \\ \underline{g}_\infty \end{bmatrix}_t + \begin{bmatrix} [\mathbf{B}]_{ss} & [\mathbf{B}]_{s1} & \cdots & [\mathbf{B}]_{sn} & [0] \\ [\mathbf{B}]_{1s} & [\mathbf{B}]_{11} & \cdots & [\mathbf{B}]_{1n} & [0] \\ \vdots & \vdots & \ddots & \vdots & \vdots \\ [\mathbf{B}]_{ns} & [\mathbf{B}]_{n1} & \cdots & [\mathbf{B}]_{nn} & [\mathbf{B}]_{n\infty} \\ [0] & [0] & \cdots & [0] & [0] \end{bmatrix} \cdot \begin{bmatrix} \underline{g}_s \\ \underline{g}_1 \\ \vdots \\ \underline{g}_n \\ \underline{g}_\infty \end{bmatrix}_t, \quad (3)$$

or in a more compact form,

$$\underline{g}_{t+1} = (\mathbf{I} + \mathbf{B}) \cdot \underline{g}_t, \quad (4a)$$

$$\underline{g}_t = \begin{bmatrix} \underline{g}_1 \\ \underline{g}_2 \\ \vdots \\ \underline{g}_k \end{bmatrix}, \quad (4b)$$

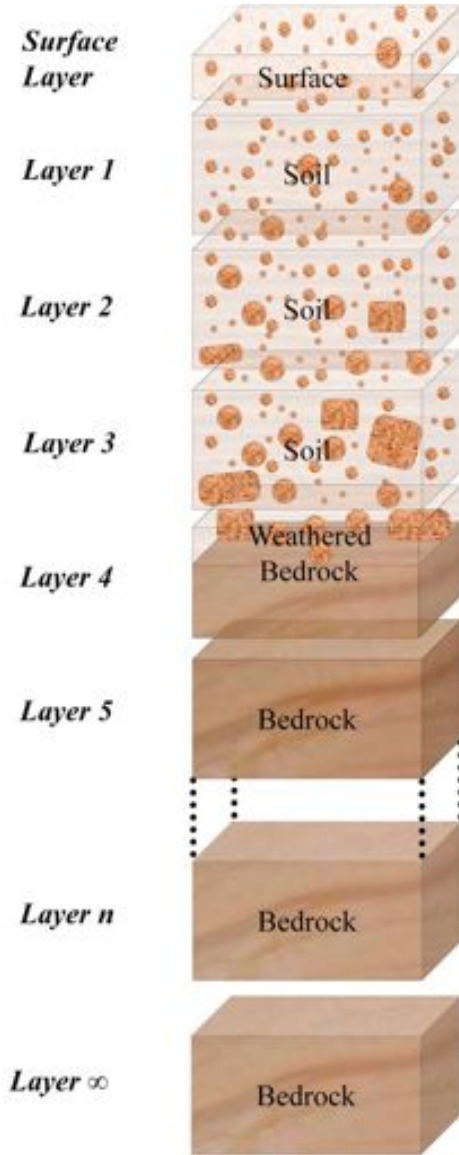


**Figure 1.** A soil-profile schematic with the profile discretized into  $n + 1$  layers. The layer thickness is user defined, the same and constant in time for all layers except the thinner surface layer. Normally, all profile layers start as bedrock (layers 5 to  $n$  in the schematic). The bedrock is weathering to soil over time (layers 1–4 in the schematic). Underlying the  $n + 1$  layers is a semi-infinite bedrock layer that resupplies layer  $n$ .

where the  $\underline{g}$  vector (the grading vector of all of the layers) in equations (3) and (4) is a concatenation of the  $\underline{g}_i$  vectors (the grading vector for layer  $i$ ), sometimes called a supervector in the modeling literature, of the grading for each of the  $n + 2$  soil layers so that  $\underline{g}$  is of dimension  $(n + 2)k$  and the double underbars are used solely to distinguish the soil-profile vector from the grading vector of a single layer in equations (1) and (2). Likewise the matrix  $\mathbf{B}$  describes not only how the grading in each individual layer evolves in isolation but also how the grading of each layer interacts with each other layer. The notation  $[\mathbf{B}]_{ij}$  indicates a  $k \times k$  matrix that describes how the grading for layer  $i$  is changed by the grading in layer  $j$  in one

time step, and  $[0]$  is a  $k \times k$  matrix filled with zeros. The matrix  $\mathbf{B}$  in equation (4), sometimes called a supermatrix in the literature, is of size  $(n + 2)k \times (n + 2)k$ . The line of  $[0]$  matrices across the bottom of  $\mathbf{B}$  indicates that the grading of the semi-infinite subsurface layer does not change with time.

[11] Typically a layer only interacts with the layers directly above and below it (though some bioturbation exceptions are discussed in Appendix A) so the  $\mathbf{B}$  matrix simplifies to

$$\mathbf{B} = \begin{bmatrix} [\mathbf{B}]_{ss} & [\mathbf{B}]_{s1} & [0] & \cdots & [0] & [0] \\ [\mathbf{B}]_{1s} & [\mathbf{B}]_{11} & [\mathbf{B}]_{12} & \cdots & [0] & [0] \\ [0] & [\mathbf{B}]_{21} & [\mathbf{B}]_{22} & \cdots & [0] & [0] \\ \vdots & \vdots & \vdots & \ddots & \vdots & \vdots \\ [0] & [0] & \cdots & [\mathbf{B}]_{n,n-1} & [\mathbf{B}]_{nm} & [\mathbf{B}]_{n\infty} \\ [0] & [0] & \cdots & [0] & [0] & [0] \end{bmatrix}, \quad (5)$$

where only the diagonal and adjacent matrices are nonzero, with all other entries zero. This general formulation ensures that any relevant physics can be easily incorporated into the mARM3D model. Below we describe the two processes used in this paper: armoring and physical weathering. Three further processes, not used here, are discussed in Appendix A: deposition, eluviation, and bioturbation. The vertical profile dynamics are parameterized by  $\mathbf{B}$ . The dynamics within each layer is expressed by a process specific matrix, which is described by equations (1) and (2).

## 2.1. Armoring Process

[12] In the armoring process material is selectively eroded from the surface layer. Since mARM3D is a mass balance model and the volume of the layers is constant with time (Figure 1), an amount of sediment equal to the eroded mass is resupplied to the surface layer from the top profile layer (layer 1; Figure 2a). The top profile layer (layer 1) is then resupplied by the layer directly below, layer 2, and so on until the bottom layer  $n$ , which is resupplied from the semi-

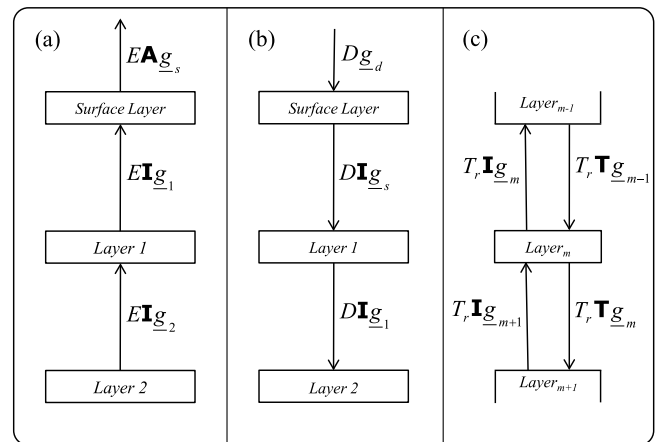


**Figure 2.** Diagram of sediment movement (in units of total mass per unit area) between profile layers for (a) erosion from the surface layer with resupply from underlying layer, layer 1; (b) deposition on the surface, which propagates down the profile (equations (A1) and (A2)); and (c) eluviation from a layer, layer  $m$ , to the layer below, layer  $m+1$ , and from the layer above, layer  $m-1$  (equation (A5)).

infinite bottom layer (layer  $\infty$ ) which for a natural soil profile we consider to be bedrock. This is how the soil profile evolves. The  $\mathbf{B}_e$  matrix (the  $e$  subscript indicates erosion) is

$$\mathbf{B}_e = \begin{bmatrix} -\frac{\Delta E}{\eta_s} \mathbf{A} & \frac{\Delta E}{\eta_s} \mathbf{I} & [0] & [0] & \cdots & [0] \\ [0] & -\frac{\Delta E}{\eta_1} \mathbf{I} & \frac{\Delta E}{\eta_1} \mathbf{I} & [0] & \cdots & [0] \\ [0] & [0] & -\frac{\Delta E}{\eta_2} \mathbf{I} & \frac{\Delta E}{\eta_2} \mathbf{I} & \cdots & [0] \\ \vdots & \vdots & \vdots & \ddots & \vdots & \vdots \\ [0] & [0] & \cdots & [0] & -\frac{\Delta E}{\eta_n} \mathbf{I} & \frac{\Delta E}{\eta_n} \mathbf{I} \\ [0] & [0] & \cdots & \cdots & [0] & [0] \end{bmatrix}, \quad (6)$$

where  $\Delta E$  is the erosion in one time step in depth units,  $\eta_i$  is the thickness of layer  $i$  (which converts sediment mass due to erosion  $\Delta E$  into a proportion of the layer mass), and  $\mathbf{I}$  is a  $k \times k$  identity matrix. This matrix formulation assumes that the grading particle distribution is defined for each size class as a proportion of the total mass. The matrix  $\mathbf{A}$  is the armoring transition matrix for the surface layer and determines the size selectivity of the sediment entrainment due to erosion.

[13] The matrix formulation in equation (6) is general and can be applied to any set of erosion physics. The erosion physics used here is the same as that used by *Cohen et al.* [2009],

$$\Delta E = e \frac{q^{\alpha_1} S^{\alpha_2}}{d_{50a}^\beta} \Delta t, \quad (7)$$

where  $e$  is the erodibility factor,  $q$  is discharge per unit width ( $\text{m}^3/\text{s}/\text{m}$ ),  $S$  is slope,  $d_{50a}$  is the median diameter (units m) of the material in the armor layer,  $\alpha_1$ ,  $\alpha_2$  and  $\beta$  are exponents which need to be calibrated, and  $\Delta t$  is the time step size. The parameter values of equation (7) we use here are the same as those of *Cohen et al.* [2009], where  $\alpha_1 = 1$ ,  $\alpha_2 = 1.2$ ,  $\beta = 1$  and  $e = 0.025$ . This equation captures the notion that erosion is reduced as the surface grading increases. The selective entrainment of fine material is done using a model where the entrainment in any grading size range is a function of the proportion of that grading range in the surface armor [*Cohen et al.*, 2009].

[14] Discharge ( $q$ ) is

$$q = \frac{rA}{A_p}, \quad (8)$$

where  $r$  is the runoff excess generation down the slope (here  $r = 4.7e^{-8} \text{ m}^3/\text{s}/\text{m}$ ),  $A$  is the upslope contributing area ( $\text{m}^2$ ) and  $A_p$  is the area of a pixel unit ( $\text{m}^2$ ).

[15] The erosion armoring transition matrix ( $\mathbf{A}$ ) entries are the amount of erosion/unit time in each of the size classes per unit of total erosion. Matrix  $\mathbf{A}$  is diagonal with the off-diagonal elements equal to zero. The diagonal elements of  $\mathbf{A}$ ,  $A_{kk}$ , are

$$A_{kk} = \begin{cases} \frac{a}{d_k^m} g_k & \text{for } k < M \\ b \frac{a}{d_k^m} g_k & \text{for } k = M, \\ 0 & \text{for } k > M \end{cases}, \quad (9)$$

where  $d_k$  is the mean diameter (units m) of size class  $k$  ( $k = 1$  is the smallest diameter grading class), the power  $m$  needs to be calibrated (here we use the same as *Cohen et al.* [2009],  $m = 4$ ),  $a$  and  $b$  are scaling factors, and  $M$  is a size threshold that determines the largest particle diameter that can be entrained in the flow as determined by the Shield stress threshold.

## 2.2. Physical Weathering Process

[16] In mARM1D weathering is only applied at the surface. In mARM3D the same physics is used to calculate physical weathering in each profile layer to yield the  $\mathbf{B}_w$  matrix (the  $w$  subscript indicates weathering):

$$\mathbf{B}_w = \begin{bmatrix} \Phi_s \Delta W \mathbf{H} & [0] & [0] & [0] & \cdots & [0] \\ [0] & \Phi_1 \Delta W \mathbf{H} & [0] & [0] & \cdots & [0] \\ [0] & [0] & \Phi_2 \Delta W \mathbf{H} & [0] & \cdots & [0] \\ \vdots & \vdots & \vdots & \ddots & \vdots & \vdots \\ [0] & [0] & \cdots & [0] & \Phi_n \Delta W \mathbf{H} & [0] \\ [0] & [0] & \cdots & \cdots & [0] & \mathbf{I} \end{bmatrix}, \quad (10)$$

where  $\Delta W$  is the amount of weathering per time step (in this paper we assumed it is constant in space and time and  $\Delta W = 1.5e^{-4}$ ) and  $\Phi_i$  is the normalized weathering factor for the layer  $i$  as a function of the layer depth relative to the surface (described in section 2.3). The matrix  $\mathbf{H}$  defines the proportion of material in size class  $k$  that contributes to smaller size classes owing to particle breakdown. A brief description of how  $\mathbf{H}$  is populated follows and is discussed in detail by *Cohen et al.* [2009].

[17] Physical weathering is calculated by breaking a parent particle into two daughter particles. As mass conservation is assumed the diameters of the daughter particles ( $d_1, d_2$ ) can be determined from the diameter of the parent particle ( $d_0$ ):

$$d_1 = \frac{d_0}{(1 + \alpha^3)^{1/3}}; d_2 = \frac{d_0}{(1 + (1 - \alpha)^3)^{1/3}}, \quad (11)$$

where  $\alpha$  is the geometry of the particle breakdown. On the basis of the results of *Wells et al.* [2008], we used, both here and in the work of *Cohen et al.* [2009], a split-in-half geometry where  $\alpha = 0.5$  which leads to  $d_1 = d_2$ .

[18] Following the operator splitting approach adopted by *Cohen et al.* [2009], the grading change for all layers in a single time step as a result of all processes is

$$\underline{\underline{g}}_{t+1} = \mathbf{B} \underline{\underline{g}}_t = \mathbf{B}_w \mathbf{B}_e \underline{\underline{g}}_t. \quad (12)$$

During the evolution of the soil profile, physical weathering will produce a finer grading while armoring will coarsen the profile by eroding fine particles from the surface causing an injection of bedrock at the bottom of the profile. These two processes compete with each other and the balance between them depends on the ratio of their rates. The profile will reach a state of dynamic equilibrium when the physical conditions result in a balance between them. Under extreme

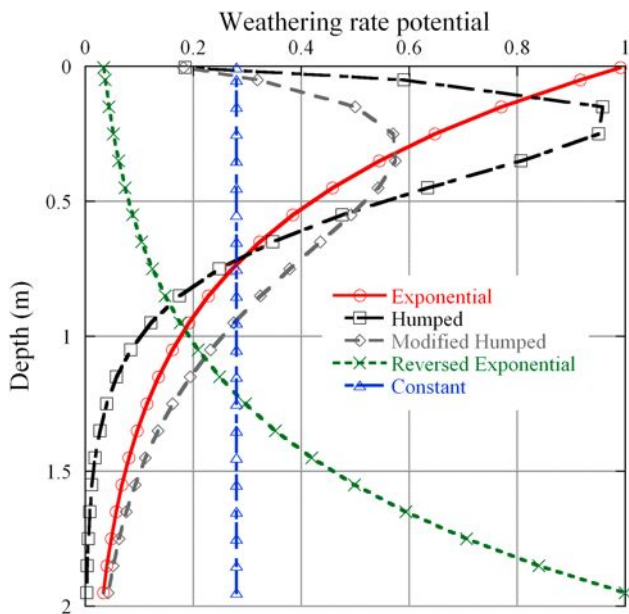


**Figure 3.** Depth-dependent weathering functions. All functions have equal cumulative weathering and vary only in the distribution down the soil profile.

erosion the soil surface can reach the lower, bedrock, boundary condition. In these high erosion rate locations (e.g., channels) soil material will be removed at a greater rate than is produced by weathering resulting in either exposed bedrock or fully armored surface. In these cases of exposed bedrock or armored surface the erosion regime becomes source-limited since erosion is limited by the supply of transportable particles.

### 2.3. Depth-Dependent Weathering Functions

[19] In this paper we use mARM3D to examine the effect of the depth dependency of weathering on the spatial and temporal trends of soil evolution. We need to distinguish between two separate, but potentially related, weathering processes. The first process is the rate at which bedrock is converted to soil, the “soil production function.” This process occurs at the bedrock-soil interface. The second process is the “soil-weathering rate,” the rate at which large soil particles break down to smaller soil particles. There are a number of studies quantifying the soil production function [e.g., Heimsath *et al.*, 1997], while there are fewer studies quantifying the soil-weathering rate [e.g., Wells *et al.*, 2006; Yoo and Mudd, 2008b].

[20] Physical weathering is considered in this study. In the simulations below the weathering rate is assumed to decrease as the soil depth increases. This assumption is based on the well established inverse relationship between soil production rate (bedrock weathering) and soil thickness. Two commonly discussed soil production functions are translated here into weathering rate depth dependency of both bedrock and soil (Figure 3): (1) exponential decline [Gilbert, 1877], where weathering rate decreases as a function of depth, and (2) the “humped” [Ahnert, 1977], where weathering rate is highest close to the surface at some nonzero depth and then decreases exponentially with depth. These

functions are implemented in the model by assigning a normalized weathering factor ( $\Phi$ ; equation (10)) to each profile layer.

[21] The conversion of the exponential and hump soil production function into depth-dependent physical weathering rate is based on the work of Wells *et al.* [2005, 2006], which found that physical weathering rates are most strongly affected by the magnitude of wetting and temperature cycles. These microclimatic fluctuations are typically strongest closer to the surface and decrease with depth. Burke *et al.* [2007] also found that saprolite chemical weathering decreased with increasing soil thickness. However, it should be noted that the rate of soil production (i.e., the conversion of bedrock to soil) is not typically considered to be the same as the rate of soil weathering (i.e., the breaking of large particles into smaller particles).

[22] The humped equation used here is a modification of the function proposed by Minasny and McBratney [2006] for their humped soil production model:

$$\frac{\partial W}{\partial t} = P_0[\exp(-\delta_1 h + P_a) - \exp(-\delta_2 h)], \quad (13)$$

where  $\frac{\partial W}{\partial t}$  is the physical weathering rate,  $P_0$  and  $P_a$  (m/yr) is the potential (or maximum) and steady state weathering rates, respectively,  $h$  (m) is the soil depth relative to the surface and  $\delta_1$  and  $\delta_2$  are constants. The values proposed by Minasny and McBratney [2006] of  $P_0 = 0.25$ ,  $\delta_1 = 4$ ,  $\delta_2 = 6$ ,  $P_a = 0.005$  are used here while  $P_0$  is modified to 0.02 (their value was 0.05) to create a function that asymptotes close to 0. Equation (14) is then normalized:

$$\Phi = \frac{\partial W}{\partial t} / M, \quad (14)$$

where  $M$  is the maximum value (i.e., the peak of the hump) in equation (13) ( $M = 0.04$ ).

[23] The exponential decline equation used here is

$$\Phi = \beta e^{-\delta_3 h}, \quad (15)$$

where  $\beta$  is constant (the maximum value;  $\beta = 1$  in this case) and  $\delta_3$  is the scaling factor. A good match was found between the weathering functions for  $\delta_3 = 1.738$ .

[24] As a contrast to the simulations above some of the following simulations are performed with a conceptualization of chemical weathering for the weathering rate. Recent literature suggests that chemical weathering of regolith and soil may have a different vertical pattern from physical weathering. Chemical weathering is strongly correlated with soil age [White and Brantley, 2003]. This suggests that chemical weathering of soil particles is strongest at the weathering front close to the bedrock [Yoo and Mudd, 2008b]. This weathering age dependency will be later examined in a sensitivity analysis (section 3.3). These simulations used the exponential and humped function for the soil production rate and a different function for the soil-weathering rate as a means of assessing the sensitivity of the soil profile to the depth dependency of the in-profile weathering process.

[25] In all of the simulations we matched the profile weathering rates to make sure that the area under the

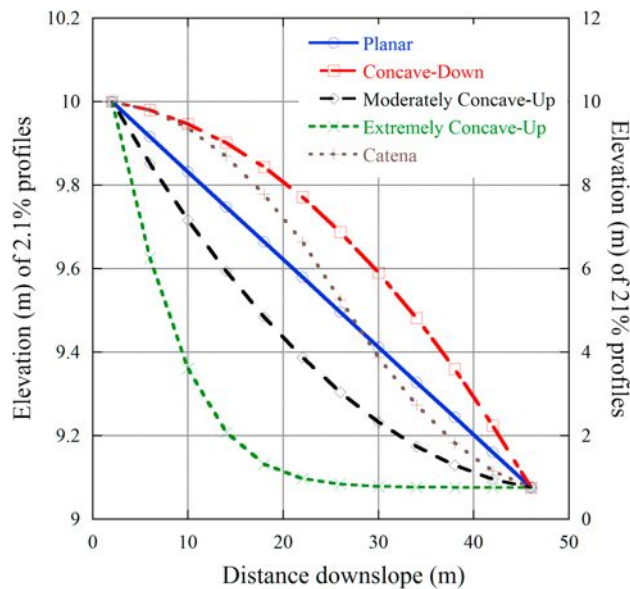


**Figure 4.** Elevation of the five hillslope profiles used for an average slope of 2.1% and 21%. In the simulations the hillslope profiles are constant with time, while the soil evolves.

weathering function curve (Figure 3) is the same. This results in equal cumulative weathering on soil particles as they are exhumed from the bedrock boundary to the surface for the functions. This means that variations in the results between the soil-weathering functions will only be due to differences in the weathering profile depth distribution and are not due to differences in cumulative weathering. The parameters values above resulted in a difference of less than 0.1% in the cumulative weathering between the weathering functions.

### 3. Hillslope-Scale Simulations of mARM3D

[26] To simplify the analysis of the results one-dimensional hillslope profiles were studied first. Soil evolution was simulated over 100,000 years using two sets of hillslope profiles. These profiles were a modified version of the 1-D hillslopes used for mARM1D [Cohen *et al.*, 2009]. The two hillslopes sets have different average slopes of 2.1% and 21%, respectively. Each set contains five longitudinal hillslope profiles (Figure 4): (1) planar, (2) concave down, (3) moderately concave up, (4) extremely concave up, and (5) catena (convexo-concave). All hillslopes were 48 m long and divided into 12 equal sized nodes downslope. The soil grading discretization used was the same as that of Willgoose and Sharmeen [2006] and Cohen *et al.* [2009]: 19 size classes from 0 to 19 mm (Table 1). The largest size class (particles larger than 19 mm) represents bedrock. The soil profile is described by 20 layers ( $n = 20$ ) each 10 cm thick. At the start of the simulations all 20 profile layers are set as bedrock while the surface layer (0.5 cm thick) is set with the initial soil-grading distribution used by Sharmeen and Willgoose [2006]. To simplify the analysis the elevation of the hillslope profiles do not evolve with time. Previous work [Sharmeen and

Willgoose, 2006] suggested that evolving both the hillslope topography and the soil only adds complexity to model interpretation, while not significantly changing the trends of the results.

[27] Two sets of simulations were carried out. The first set used the same function for both the soil production and soil-weathering functions, both declining with depth. These were designed to simulate physical weathering processes. The second set of simulations used the same soil production function but a different soil-weathering function. These were designed to understand the interdependency of the soil profile, soil production rate and the soil-weathering rate, and as a simple conceptualization of chemical weathering. Within each set of simulations we used two different soil production functions, hereinafter referred to as “exponential” and “humped” (section 2.3).

#### 3.1. Identical Soil Production and Soil-Weathering Functions

[28] Figures 5 and 6 show the equilibrium surface  $d_{50}$  distribution for the five hillslope profiles. The planar hillslopes resulted in downslope coarsening owing to the increased erosion with increasing contributing area downslope. This trend is even stronger for the concave-down profile owing to the increasing slope downslope. The extremely concave-up profile resulted in downslope fining owing to the significant decrease in slope downslope which reduced erosion. In the moderately concave-up profile, grading is similar at the top and the bottom of the hillslope with only a small change in  $d_{50}$  range down the hillslope (0.5 mm, 2.1% profiles; 3 mm, 21% profiles; Figure 5). This relative homogeneity in soil grading suggests a balance between area, slope and soil grading.

[29] These results are qualitatively similar for both the 2.1% and 21% simulations of the exponential simulation (Figures 5a and 5b, respectively). The differences between the two slopes are in the intensity of the process and the resulting  $d_{50}$  values, which are coarser for the steeper slopes, rather than any fundamental change in the patterns of soil distribution down the hillslope.

**Table 1.** Soil Grading Size Classes and Initial Surface Grading Used in This Paper

Diameter $d$ (mm)	Mass Retained (%)
0.0	0.35
0.016	0.35
0.032	0.35
0.0475	0.35
0.063	0.75
0.0795	0.75
0.096	0.75
0.111	0.375
0.118	0.375
0.125	0.575
0.156	0.575
0.187	1.15
0.25	10.2
0.5	9.6
1.0	12.5
2.0	16.4
4.0	20.0
9.5	24.6
19.0	0.0

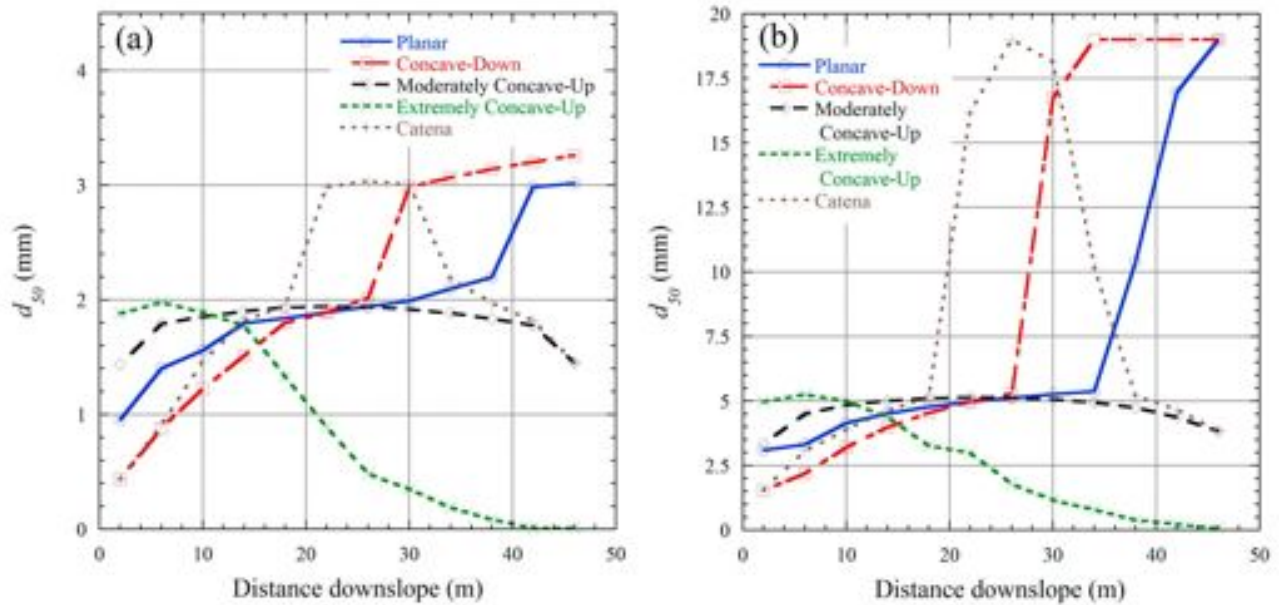


**Figure 5.** Equilibrium surface  $d_{50}$  distribution for (a) 2.1% total slopes and (b) 21% total slopes, using the exponential weathering function.

**3.2. Effect of the Form of Soil Production Function**

[30] In the lower slope simulations (2.1%) the exponential and humped weathering functions resulted in similar surface distribution trends in all five hillslope profiles (albeit slightly higher  $d_{50}$  values for the humped; Figures 5a and 6a, respectively). In contrast, the high slope simulations (21%) resulted in some notable differences for the two weathering functions (Figures 5b and 6b) for the planar, concave-down and catena profiles. In the exponential simulation (Figure 5b) the  $d_{50}$  in these three hillslope profiles has spiked to the

maximum  $d_{50}$  value of 19 mm (the size of the largest soil grading class; Table 1) in the most erosive part of the hillslope (downslope for the planar and concave down and midslope for the catena profile). This did not occur in the two concave-up profiles in the exponential simulation, nor did it occur in any of the humped simulation profiles. To understand the cause of these differences the evolution of surface  $d_{50}$  was plotted.

[31] The surface  $d_{50}$  evolution plot of the 21% planar profile (Figure 7) show that the four upslope nodes have

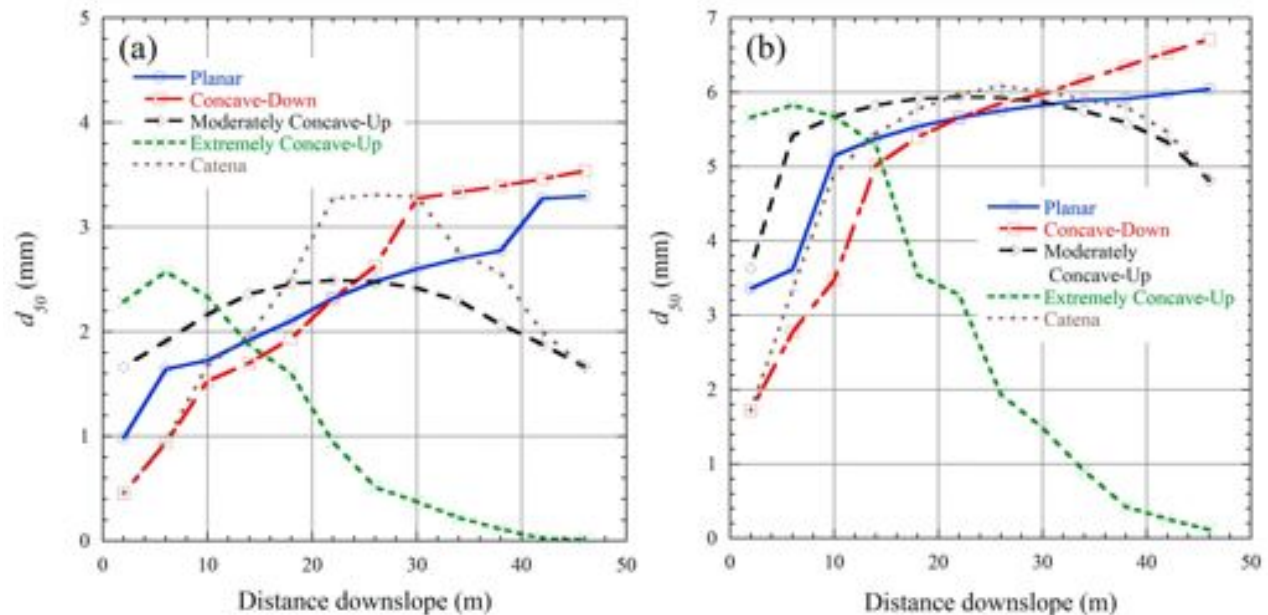


**Figure 6.** Equilibrium surface  $d_{50}$  distribution down the profiles for (a) 2.1% total slopes and (b) 21% total slopes, using the humped weathering function.

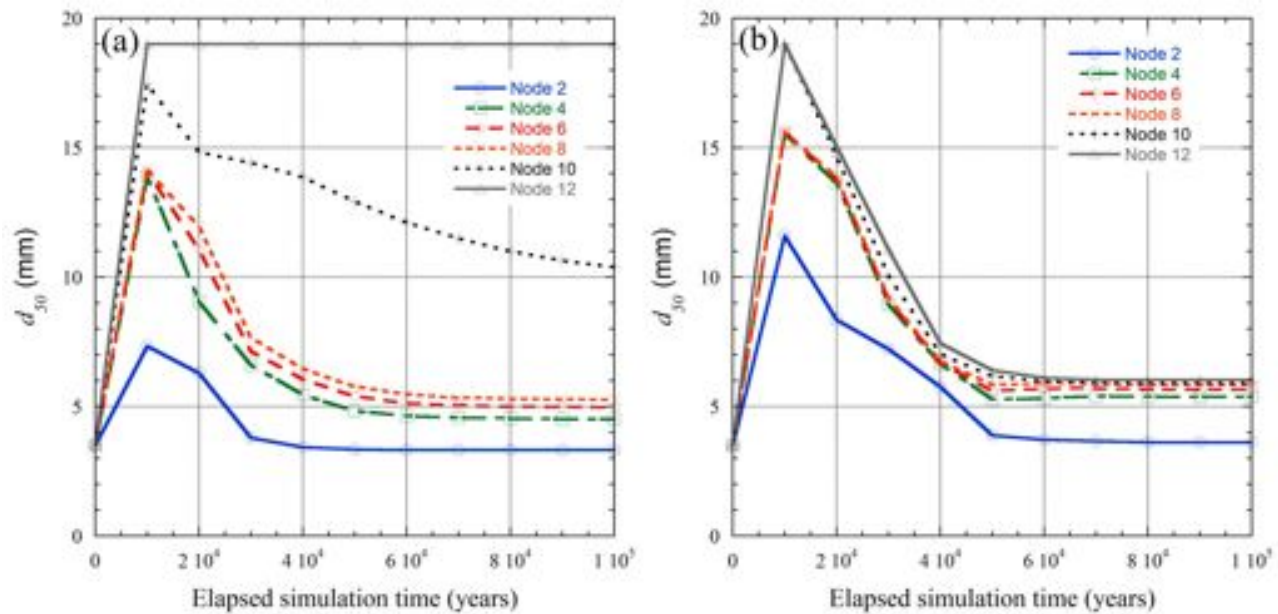


**Figure 7.** Surface grading ( $d_{50}$ ) evolution over a 100,000 year simulation of two planar hillslope profiles with total slope of 21% using the (a) exponential weathering function and (b) humped weathering function. Node numbers increase in the downstream direction.

very similar evolution trends in the grain size and equilibrium values for both weathering functions. The only notable difference for these nodes is that the humped simulation resulted in a steeper increase in  $d_{50}$  values at the start of the simulation. This initial spike in the grading is due to the rapid armoring of the surface. The subsequent fining of the grading occurs as the weathering starts to become dominant.

[32] The most significant differences between the two weathering functions are at the two downslope nodes. The most downslope node had the maximum  $d_{50}$  value (19 mm) at the initial surface armoring stage in both simulations (Figures 8a and 8b). However, for the exponential simulation (Figure 7a) the  $d_{50}$  remained 19 mm while in the humped simulation (Figure 7b) the value decreased as occurred for all of the hillslope. Node 10 shows an intermediate trend as its  $d_{50}$  value is decreasing for the exponential simulation but much less than in the humped simulation. These differences show that the more erosive nodes (where transportability is high) in the exponential simulation reached a source-limited (armor dominated) erosion regime while their equivalents in the humped simulation reached a transport-limited (weathering dominated) regime. A source-limited erosion regime means that the weathering is not intense enough to balance the erosion. This results in either exposed bedrock or an armored surface.

[33] The parameters of the weathering functions (Figure 3) were chosen to ensure that the cumulative weathering from the bedrock-soil interface to the surface was identical and that the weathering profiles varied only in their distribution through the vertical profile. The most significant differences between the exponential and humped functions are (1) that the surface weathering rate is much higher in the exponential ( $\Phi = 1$  versus  $\Phi = 0.2$  in the humped function; Figure 3) and (2) that the weathering rate in the upper subsurface layers is

higher in the humped. The fact that some nodes only reached a source-limited erosion regime when using the exponential function cannot be explained by the first difference between the two weathering functions (point 1 above). This is because higher surface weathering rates will result in finer rather than coarser grading which is less likely to result in a source-limited erosion regime. This leaves point 2 as the most likely explanation for why the humped equation did not result in a source-limited erosion regime.

[34] Figure 8 is a three-dimensional plot of the  $d_{50}$  distribution versus depth and hillslope position for the planar profile with 21% slope for the two weathering functions. Both simulations show a trend of decreasing  $d_{50}$  values from the bottom of the profile upward followed by a sharp increase at the surface. The main differences between the two hillslope profiles are that the humped function resulted in a thicker fine-grained subsurface layer. We believe that this layering has prevented the surface becoming source-limited.

[35] In order to confirm that these results are not merely an artifact of the parameters used in the humped function, the planar profile is simulated using a modified humped equation ( $P_0 = 1.0$ ,  $P_a = 0.08$ ,  $\delta_1 = 2$ ,  $\delta_2 = 4$ ; Figure 3). The modified equation retains the same surface and cumulative weathering rate as the original and varies only in the distribution down the profile. The results reveal that the trends and equilibrium values are similar to the original. They did, however, require about 50% longer time to reach equilibrium. This confirms that it is the humped depth profile, not the weathering rate nor the exact location of the hump within the profile of the weathering function that is important.

### 3.3. Soil Thickness

[36] In mARM3D the soil thickness is calculated by subtracting the volume of bedrock (assumed to be that

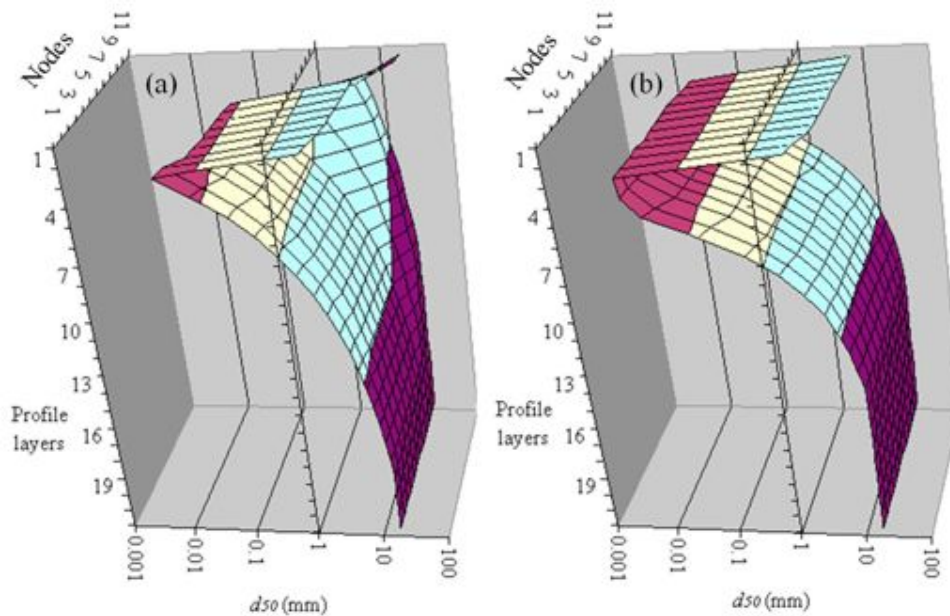


**Figure 8.** Profile  $d_{50}$  distribution down the 21% slope planar profile using the (a) exponential weathering function and (b) humped weathering function. Node numbers increase in the downstream direction.

material in the largest grading class) from the total volume of the simulated soil profile. Figure 9 displays the distribution of soil thickness in the five hillslope profiles with a slope of 21% for the exponential simulation. In all five profiles, the equilibrium soil thickness distribution shows strong negative correlation with surface grading ( $d_{50}$ ; Figures 5b and 9). The reason for this negative correlation is that as erosion increases (relative to weathering) the surface becomes coarser while relatively more soil is removed from the profile resulting in a thinner soil. This negative correlation between soil grading and thickness is likely to be valid only on the erosive parts of a natural hillslope as deposition may lead to a positive correlation. This issue will be examined in the future work when deposition (described in section A1) will be simulated.

[37] For the exponential profile the planar, concave-down and catena profiles all reached the maximum surface  $d_{50}$  value of 19 mm in several nodes (Figures 5b and 9). These nodes resulted in lower soil thickness compared to the rest of the hillslopes (100 cm compared to about 150 cm; Figure 9). However, the fact that there is a significant amount of soil in these nodes indicates that the high surface grading is not due to total removal of soil from the profile (i.e., there is no exposed bedrock), rather it is as a result of a fully developed surface armor. This can also be observed in the 3-D profile plot (Figure 8a) where the most downslope node (number 12) has a very high surface  $d_{50}$  but still has some weathered material in its subsurface layers.

**3.4. Effect of the Soil-Weathering Function**

[38] The simulations described so far examined the differences in the soil profile and distribution in space as a result of two competing hypotheses for the bedrock to soil conversion rate at the base of the soil profile (i.e., the “soil production function”). In these simulations we assumed that

the soil-depth dependence of the soil production function was the same as the depth dependence of the soil particle weathering rate (i.e., the rate at which large soil particles break into smaller soil particles). In this section we examine the importance of this latter assumption by examining two depth distributions of soil particle weathering rates (hereinafter referred to simply as “weathering profiles”) that contrast with the exponential decline with soil depth in section 3.3.

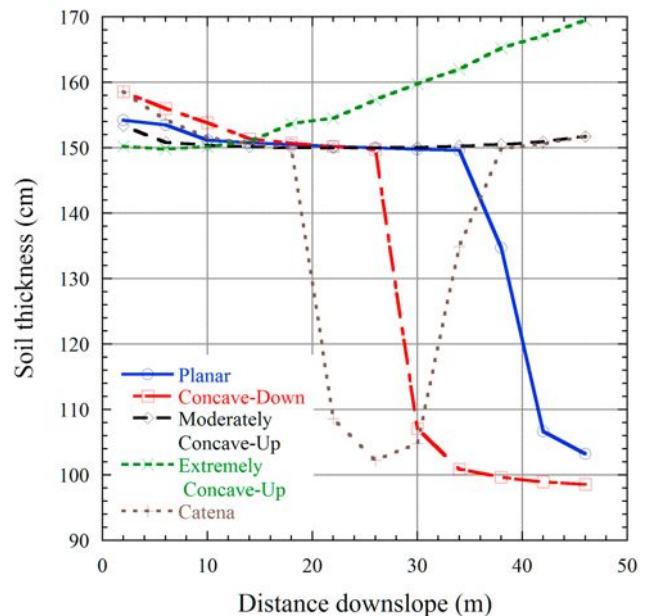


**Figure 9.** Soil thickness distribution for the 21% slopes for the exponential weathering function simulation.

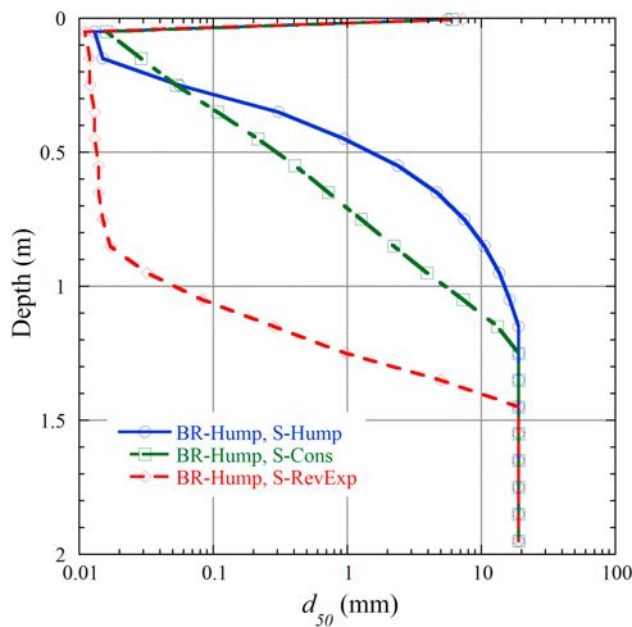


**Figure 10.** Equilibrium profile for the middle of the hillslope with the three combinations of bedrock (BR) and weathering profiles (S). The weathering profiles are as follows (Figure 3): Hump, the humped function decreasing with depth; Cons, constant weathering rate with depth; and RevExp, the reverse exponential exponentially increasing with depth.

[39] 1. The first weathering profile is a constant weathering profile where the weathering rate is independent of soil depth. As we will see, this weathering profile is useful for elucidating the process dependencies of the soil profile.

[40] 2. The second weathering profile has a weathering rate which increases exponentially with depth (hereinafter “reverse exponential”). This profile captures the hypothesis that the weathering rate of a particle should be a function of the time since the particle was converted to soil from rock (i.e., particle age), and is a function of chemical reactivity. This profile then qualitatively captures how chemical weathering influences soil-profile evolution. It allows us to start to extend the conclusions of this paper from a singular focus on physical weathering to some forms of chemical weathering.

[41] These simulations were done with both of the humped and exponential soil production functions (described in section 2). The results for the humped function are presented in Figures 10 and 11. The results for the exponential soil production function are qualitatively similar and will not be discussed further. For comparability, the rate coefficients of the three weathering profiles have been normalized so that for a 2 m deep soil all particles will be subjected to the same cumulative weathering. The only difference is the depth distribution of the weathering. The humped weathering profile (Figure 10) is identical to that used previously (Figure 8).

[42] For the constant weathering profile the  $d_{50}$  distribution with depth in Figure 10 is linear. This reflects the

constant weathering rate with depth, which means that, for example, it takes the same time to break down a 10 mm particle to 1 mm fragments as it does a 1 mm particle to 0.1 mm. The constant weathering profile highlights that the slope of the  $d_{50}$  line with depth is simply proportional to the weathering rate at that depth.

[43] For the reverse exponential we see that the rate of breakdown is fastest near the base of the soil profile, which is as expected given the weathering profile and the observation that the slope of the  $d_{50}$  profile is proportional to the weathering rate at that depth. The convergence to a diameter of 0.01 mm reflects a threshold applied in the model that says that below a particle diameter threshold (typically at or near the rock crystal size) the weathering rate drops markedly.

[44] The results are suggestive of soil layering or horizons with marked changes in certain parts of the profile that separate other more homogeneous parts of the profile. While in Figure 10 we show only one profile at one point along a hillslope, these results are observed on all positions along the hillslopes.

[45] Figure 11 shows the  $d_{50}$  of the surface down the hillslope. Compared with the marked differences between the soil profiles in Figure 10 the effect of the differences between the weathering profiles down the hillslope are less dramatic. The reason for this is that we normalized the profiles so that for a 2 m deep soil profile the cumulative weathering of the three profiles was the same. If the soil thickness down the hillslope was fixed at 2 m, the surface  $d_{50}$  would be the same for all three profiles. That they vary between the weathering profiles is simply a reflection that the soil is not 2 m deep all the way down the hillslope.

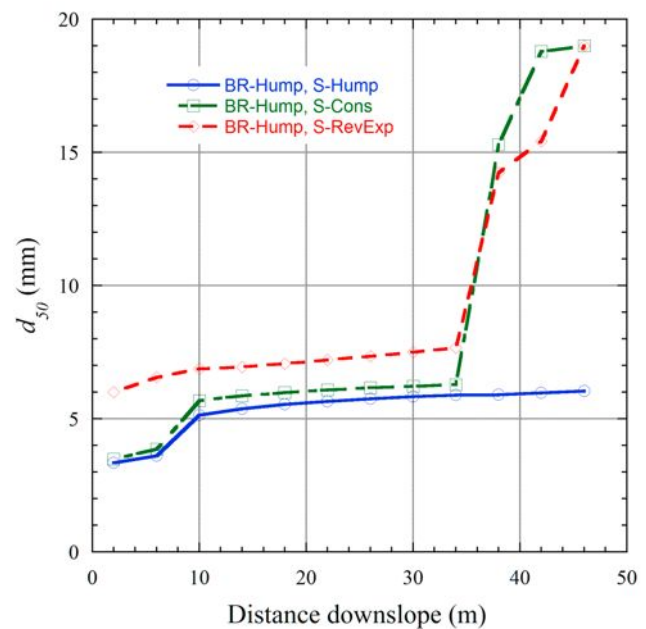


**Figure 11.** Equilibrium surface  $d_{50}$  distribution down the planar hillslope with 21% slope with the three combinations of bedrock and soil-depth-dependent weathering functions. The functions are in Figure 3.

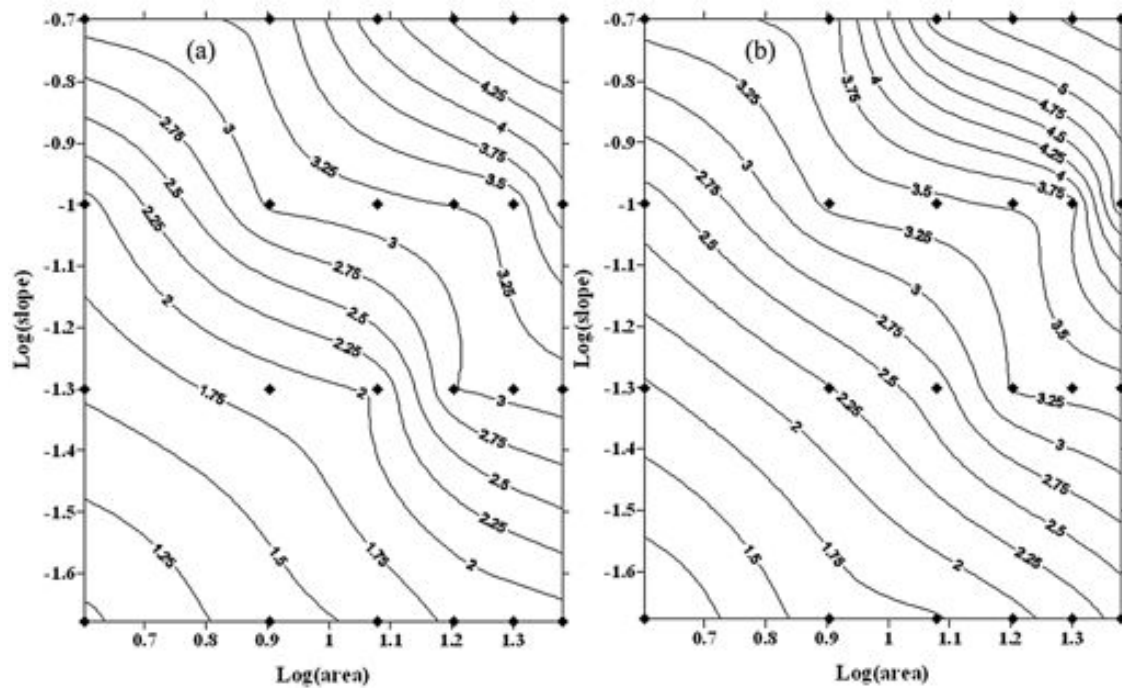


**Figure 12.** Contour map of  $d_{50}$  (mm) interpolated from 24 nodes (diamonds) simulated by mARM3D (slope lengths of 4, 8, 12, 16, 20, and 24 m and gradients of 2.1%, 5%, 10%, and 20%) using the exponential weathering function. The humped simulation results are nearly identical.

These results are consistent with those in Figure 6 when comparing the humped and exponential weathering profiles. Figure 11 emphasizes that for the surface grading it is the cumulative weathering that the surface particles have been exposed to over their life that is critical, and not the depth and/or time at which the particles have been weathered. The reason for this is straightforward. For the reverse exponential profile the weathering is concentrated at the bottom of the soil profile so the cumulative weathering of a particle is very insensitive to soil thickness because reductions in soil thickness only remove the low weathering rate tail of the exponential curve. This is also true of the exponential and humped profiles. Thus we conclude that the grading of the soil delivered to the surface will be insensitive to the depth distribution of the weathering profile and to first order only a function of the rate constant on the process itself.

[46] This result hints at an interesting conclusion. This conclusion is that the depth dependence of the weathering profile is not important in the development of organization or catena in surface soil grading and that this organization must result from other processes. Furthermore, if the weathering rate (i.e., the rate coefficient on the front of the weathering profile equation) does not change down the hillslope (e.g., it is independent of soil moisture) then the weathering rate is also not responsible for surface soil organization.

### 3.5. Area-Slope- $d_{50}$ Relationship

[47] In the mARM1D study [Cohen *et al.*, 2009] a log-log linear relationship between area, slope and  $d_{50}$  (hereinafter,  $ASd$ ;  $d_{50} = c \cdot Area^\alpha \cdot Slope^\beta$ ) was discovered after simulating four hillslopes with different slopes. This analysis was repeated for four weathering rates and only  $c$  was found to be dependent on the weathering rate. The  $ASd$  relationship

fitted all of the simulations very well and the scaling parameters  $\alpha$  and  $\beta$  did not change significantly with changes in process parameters. This analysis was repeated with mARM3D using the exponential and humped weathering functions. The resulting contour map (Figure 12) and correlation analysis (Table 2) were similar to each other, even for different weathering function. Furthermore, the results correspond well with the mARM1D simulations (Table 2). The contour maps (Figure 12) have similar trends, the correlation equation parameters fall in the same range, and the  $\alpha/\beta$  ratio is comparable (Table 2). These findings emphasize the robustness of the  $ASd$  relationship to changes in in-profile pedogenic processes.

[48] It should be noted that no node reached a source-limited regime, which would have significantly changed the  $ASd$  relationship. They are therefore limited to relatively moderate erosion rates for soil-mantled landscapes. These conditions may be classified as transport-limited erosion regimes associated with hillslope processes as opposed to source-limited erosion regime associated with channels. The  $ASd$  analysis suggests that for transport limitation the  $ASd$  relationship is robust and that the addition of a soil-profile component (i.e., mARM3D versus mARM1D) does not change the link between the scaling behavior of soil grading and topography. This suggests a general solution for the  $ASd$  relationship might have usefulness for digital soil mapping and environmental modeling.

## 4. Landscape Simulations

[49] The results above are for one-dimensional hillslopes without flow convergence and divergence. Landscape simulations were carried out using mARM3D to explore the

**Table 2.** Parameters of the Area-Slope- $d_{50}$  Multiregression Analysis, Where  $d_{50} = cA^\alpha S^\beta$ , for the Exponential and Humped Weathering Functions

	Weathering Function/Rate	$c$	$\alpha$	$\beta$	$\alpha/\beta$
mARM3D	Exponential	3.32	0.36	0.43	0.84
	Humped	3.65	0.38	0.43	0.88
mARM1D [Cohen et al., 2009]	1.0	3.19	0.7	0.7	1.0

impact of more complex surface flow geometries. A DEM of an artificial mound was used [from Willgoose and Riley, 1998]. It covers approximately 0.76 km<sup>2</sup> at a pixel resolution of 8 m. This DEM is used here as a general example of a complex landform. It is not intended to realistically simulate soil evolution of a specific site; rather it is to understand the potential effect of a more complex landform. The initial soil grading and soil thickness are the same as the hillslope simulations.

[50] Figure 13 displays the equilibrium surface  $d_{50}$  maps after 50,000 years for the exponential and humped simulations. As expected the maps demonstrate a coarser grading in the high-slope areas (i.e., higher-density contours) and high contributing areas regions (midnorth and midwest sections). The exponential simulations had lower  $d_{50}$  values with an average of 2.85 mm compared to 3.22 mm in the humped simulation. On the other hand, the exponential simulation resulted in a larger number of source-limited

pixels (1.61% compare to 0.55% in the humped simulation). Other than that, as for the hillslope simulations, the difference between the humped and exponential simulations is small.

### 5. Discussion

[51] The mARM3D model is designed as a comprehensive landscape-pedogenesis framework. The innovation of mARM3D, compared to existing models, is its ability to calculate the interaction between landscape and profile processes in a spatially, temporally and physically explicit way. This was made possible by its novel use of transition matrix numerics, which improve its computational efficiency by a factor of 10<sup>4</sup> compared to traditional physically based models [Cohen et al., 2009]. The computational efficiency and modularity of mARM3D allowed detailed simulations of complex landscape-pedogenesis interactions

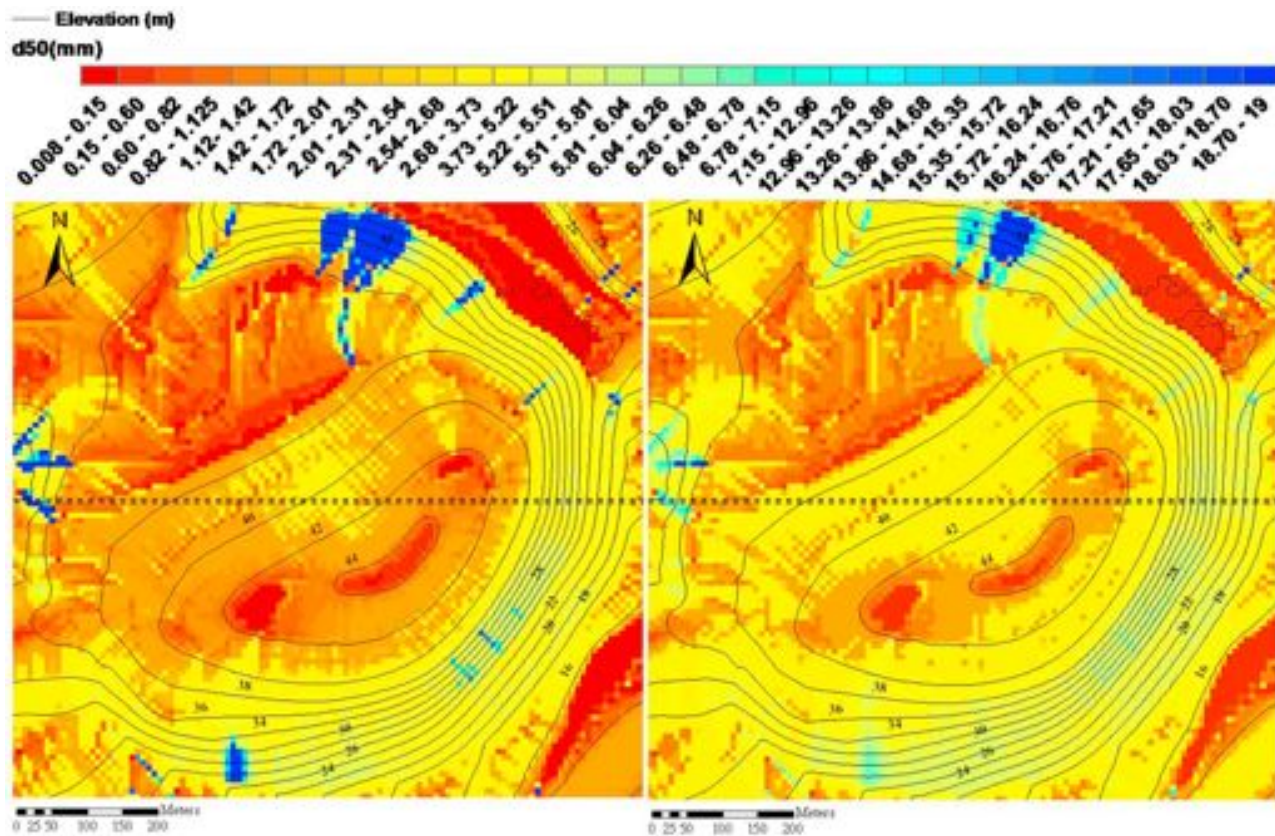


**Figure 13.** Close to equilibrium (after 50,000 years) surface  $d_{50}$  maps of an artificial mound site using the (left) exponential weathering function and (right) humped weathering function. The dark blue areas are source-limited where the surface armor is fully developed.

over large spatial and long time scales. Even though mARM3D can model complex landscape-pedogenesis interactions (as demonstrated here and in the work of *Cohen et al.* [2009]) in this paper we simulated just two pedogenic processes, armoring and physical weathering. We did so in order to allow clearer interpretation of causal relationships in the results. The implications of these simplifications are that (1) the results should only be interpreted for the erosive sections of the hillslope, as deposition is not simulated, and (2) caution should be applied when transferring the results to natural environments as potentially important processes were not included (e.g., biogeochemical, translocation, diffusion).

[52] Subject to these caveats, we used the mARM3D model to study the effect of bedrock- and soil-weathering dynamics on soil-profile and surface pedogenesis. Various depth-dependent weathering functions were simulated. The results clearly showed that the grading of the soil profile through depth is strongly affected by the depth dependency of the functions used to describe soil and bedrock weathering (Figures 8 and 10). This is an important insight as many soil properties, primarily hydrological properties, are strongly affected by the soil-profile grading distribution. It implies that in order to reliably calculate the vertical properties of soils we need to accurately describe the weathering function.

[53] The sensitivity analyses in section 3 showed that different combinations of soil- and bedrock-weathering functions strongly affect the profile grading distribution. The results suggest that the shape of the bedrock-weathering function (e.g., exponential decline or the humped in section 3.2) controls the equilibrium soil thickness while the shape of the soil-weathering function controls the distribution of soil grading down the profile. Our results suggest a mechanism whereby both chemical and physical soil weathering can create layering (i.e., horizons) in the soil profile. This is an aspect of the model that deserves further investigation as the development of horizons within the soil profile is considered by many soil scientists to be one of the more important outcomes of soil pedogenesis (A. B. McBratney, personal communication, 2010).

[54] Despite the sensitivity of the profile evolution to the shape of the weathering function, its effect on equilibrium surface soil grading was found to be small. The equilibrium soil grading was primarily a function of the weathering rate, not of the distribution down the soil profile. The hillslope-scale results showed that different weathering functions can lead to different erosion regimes, particularly in the more erosive sections of the hillslope. However, the landscape-scale results showed that this typically only influences a very small portion of the landscape (about 1%). We therefore conclude that the equilibrium surface soil grading is relatively insensitive to the profile weathering functions and is primarily a function of the process rate coefficient.

[55] *Heimsath et al.* [1997] argued that differences between the exponential and humped soil production functions make little difference to modeling. The low sensitivity, found in this paper, of equilibrium surface grading to the shape of the weathering function is generally consistent with their argument. However, the results here showed that this argument is only valid for surface conditions. This does not imply that it is unnecessary to simulate profile processes in order to

calculate surface conditions. Other pedogenesis processes (such as discussed in Appendix A) may have a more complex effect on surface evolution (this will be examined in our future work) and might therefore be important for predicting the spatial distribution of natural soils.

[56] *Cohen et al.* [2009] discovered a log-log linear relationship between catchment area, slope and soil surface  $d_{50}$ . They only examined surface weathering and armoring processes. In this paper we reexamined this relationship with the full soil-profile model of mARM3D and found the same relationship. This suggests that the log-log linear relationship between area, slope and  $d_{50}$  is a robust result. In particular, this paper found that equilibrium surface grading is insensitive to the shape of the weathering function so that the full profile modeling in mARM3D had little impact on the spatial organization of the surface soil grading. This result indicates that surface soil grading across a catchment could potentially be estimated based solely on area and slope. This may be of great use in a variety of applications such as geomorphological modeling (e.g., landform evolution) where the soil grading distribution could then be easily calculated without the need for pedogenic modeling. This would also be of value in the field of digital soil mapping for better describing the topographic aspects of soil distribution. This idea is a promising focus for future work.

## 6. Conclusions

[57] The novel, computationally efficient, transition matrix algorithm (described here and by *Cohen et al.* [2009]) allowed us, for the first time, to explicitly couple soil profile and surface processes at a landscape scale. The resulting mARM3D model can simulate soil evolution from bedrock to fully developed soils at large spatial scale, at fine spatial resolution, and over long time scales.

[58] Here mARM3D was used as a virtual laboratory to explore the effect of depth-dependent weathering functions (Figure 3) on soil evolution at hillslope and landscape scales. The results showed that the shape of the weathering function had a significant effect on vertical soil distribution (i.e., profile soil grading arrangement). Furthermore it was shown that these differences can lead to changes in the erosion regime in parts of the hillslope. However, despite these important differences, the overall equilibrium surface grading was very similar for all the weathering functions. We therefore conclude that the exact distribution of the weathering function with soil depth used is important for describing the vertical soil distribution but less important for equilibrium surface grading. The equilibrium soil grading at the surface is primarily a function of the weathering rate coefficient.

[59] The soil-topography relationship (area-slope- $d_{50}$  correlation) was examined and was found to be similar even with markedly different weathering functions. In addition, these results were consistent with our previous results using mARM1D. This shows that the scaling of the area-slope- $d_{50}$  relationship is relatively unaffected by profile processes. If a general solution to the soil-topography relationship could be analytically derived it would be potentially useful in a variety of soil and geomorphic applications.

[60] In this paper we used mARM3D to simulate two basic landscape-pedogenesis processes (armoring and physical weathering). A sensitivity study using a crude chemical

weathering analog showed that chemical weathering will only be important for predicting the soil-profile properties, not the soil surface properties. Additional processes (e.g., chemical weathering, translocation) will be integrated in the future. This will allow for more complex studies of soil evolution processes and relationships. Our vision is that with additional development and validation mARM3D will provide insight into the quantitative processes leading to soil spatial organization and a detailed description of functional soil properties for environment models.

## Appendix A: Additional Pedogenesis Processes

[61] As discussed throughout this paper, the simulations in this paper include only two processes: armoring by fluvial erosion, and physical weathering. This was done to simplify the explanation and analysis of the results. However, the natural evolution of soil involves other processes. Integration of additional processes is best done gradually to facilitate better understanding of causality. Below we illustrate how three additional processes can be incorporated into mARM3D: (1) deposition, (2) eluviation/illuviation, and (3) bioturbation. These processes are presented here to allow future implementation in mARM3D or other models, and to demonstrate the generality of the state-space matrix architecture of the mARM3D model.

### A1. Sediment Deposition

[62] For deposition, sediment of a known grading is added to the surface (Figure 2b). Material is then redistributed down into the profile and is expressed as

$$\mathbf{B}_d = \begin{bmatrix} -\frac{D}{\eta_s} \mathbf{I} & [0] & [0] & [0] & \cdots & [0] \\ \frac{D}{\eta_1} \mathbf{I} & -\frac{D}{\eta_1} \mathbf{I} & [0] & [0] & \cdots & [0] \\ [0] & \frac{D}{\eta_2} \mathbf{I} & -\frac{D}{\eta_2} \mathbf{I} & [0] & \cdots & [0] \\ \vdots & \vdots & \vdots & \ddots & \vdots & \vdots \\ [0] & [0] & \cdots & \frac{D}{\eta_n} \mathbf{I} & -\frac{D}{\eta_n} \mathbf{I} & [0] \\ [0] & [0] & \cdots & \cdots & [0] & [0] \end{bmatrix}, \quad (\text{A1})$$

where  $D$  is the deposition in one time step (defined positive for deposition). Note that for deposition there is one extra step because equation (A1) does not account for the grading of the deposited material which must be modeled with an extra step using equations (1) and (2) and is applied to the surface layer only:

$$\mathbf{g}_{sa} = \mathbf{g}_{sb} + \frac{D}{\eta_s} \mathbf{g}_d, \quad (\text{A2})$$

where the subscripts  $a$ ,  $b$  and  $d$  refer to after deposition, before deposition, and deposited sediment, respectively. In the bottommost layer if all bedrock has been “pushed down” excess materials will be pushed into a semi-infinite bedrock sublayer.

### A2. Eluviation/Illuviation

[63] Eluviation is the mechanical translocation of fine particles (primarily clay) down the profile by water and illuviation refers to the accumulation of these particles [Ollier and Pain, 1996]. Legros and Pedro [1985] used a simple eluviation/illuviation model to describe particle size distribution in soil profiles. Their model displaced particles smaller than  $2 \mu\text{m}$  and accumulated them at the bottom of the profile. This mechanism can be implemented in mARM3D by transferring a portion of the smaller than  $2 \mu\text{m}$  size classes (all classes  $k < 2 \mu\text{m}$ ) from a profile layer ( $l$ ) to the one below it ( $l + 1$ ):

$$\mathbf{g}_k^{l+1} = \begin{cases} \mathbf{g}_k^{l+1} + \lambda_k \mathbf{g}_k^l & k < 2 \mu\text{m} \\ \mathbf{g}_k^{l+1} & k > 2 \mu\text{m} \end{cases}, \quad (\text{A3})$$

$$\sum_k \lambda_k = 1, \quad (\text{A4})$$

where  $\lambda$  is the eluviation rate.  $\lambda$  is expressed as the proportion of the layer  $k$  that is eluviated in one time step or in units of depth/time step it is  $\lambda\eta$  where  $\eta$  is the thickness of the layer being modeled. The displaced material from the upper layers will be then resupplied by transferring an equivalent portion of material upward similar to the erosion resupply mechanism described above. It is

$$\mathbf{B}_{ie} = \begin{bmatrix} -\frac{\lambda}{\eta_s} \mathbf{T} & \frac{\lambda_r}{\eta_s} \mathbf{I} & [0] & [0] & \cdots & [0] \\ \frac{\lambda}{\eta_1} \mathbf{T} & -\frac{\lambda}{\eta_1} (\mathbf{T} + \mathbf{I}) & \frac{\lambda}{\eta_1} \mathbf{I} & [0] & \cdots & [0] \\ [0] & \frac{\lambda}{\eta_2} \mathbf{T} & -\frac{\lambda}{\eta_2} (\mathbf{T} + \mathbf{I}) & \frac{\lambda}{\eta_2} \mathbf{I} & \cdots & [0] \\ \vdots & \vdots & \vdots & \ddots & \vdots & \vdots \\ [0] & [0] & \cdots & \frac{\lambda}{\eta_n} \mathbf{T} & -\frac{\lambda}{\eta_n} (\mathbf{T} + \mathbf{I}) & \frac{\lambda}{\eta_n} \mathbf{I} \\ [0] & [0] & \cdots & \cdots & [0] & [0] \end{bmatrix}. \quad (\text{A5})$$

Each layer transfers a portion of the soil in the grading classes which are smaller than  $2 \mu\text{m}$  to the layer immediately below it (Figure 2c). The matrix  $\mathbf{T}$  defines what the grading distribution is of the material that is moved down. This downward movement of  $< 2 \mu\text{m}$  sediment is balanced with an upward movement of an equal mass of sediment with a grading distribution equal to the full grading distribution of the layer below (Figure 2c). Over time this process will lead to accumulation of material smaller than  $2 \mu\text{m}$  in the lowest layer. The challenge in modeling eluviation/illuviation is to determine the depth dependency of  $\lambda$  and its spatiotemporal characteristics.

### A3. Bioturbation

[64] Biotic activity and its influence on soil evolution and distribution processes can be extremely complex. Plants, animals and fungus can change weathering rates (both physical and chemical) and soil properties in the profile [Paton et al., 1995]. Since biological activity is strongly

influenced by environmental conditions, the rate and nature of these processes can vary in both space and time. *Salvador-Blanes et al.* [2007] simulated the effect of earthworms/ants/termites activity in their soil-profile model. They did this by moving a portion of the particles smaller than 2 mm from the subsurface layer to the surface. They calculated the amount of material removed from each profile layer as a function of the mean depth of the layer relative to the surface ( $h$ ), soil thickness and potential biological activity. Their depth-dependent translocation rate ( $\Psi$ ) (units are mass/m<sup>2</sup> plan area/m height/time)

$$\Psi = \Psi_0 e^{-ch}, \quad (\text{A6})$$

where  $c$  is constant (they used  $c = 10$ ) and  $\Psi_0$  is the rate at zero depth. Equation (A6) is presented simply as an example of how bioturbation rate might vary with depth because the formulation below is independent of the exact form of equation (A6).

[65] In mARM3D bioturbation can be expressed as a transition of a portion ( $B_r$ - bioturbation rate) of size classes smaller than 2 mm from each layer, within the biotic activity depth, to the surface layer. This is similar to eluviation except that material is moved directly to the surface rather than to the adjacent soil layer so that

$$\mathbf{B}_b = \begin{bmatrix} -\frac{\sum_i B_{ri}\Psi_i}{\eta_s} & \frac{B_{r1}\Psi_1}{\eta_s} \mathbf{C} & \frac{B_{r2}\Psi_2}{\eta_s} \mathbf{C} & \dots & \frac{B_{rm}\Psi_m}{\eta_s} \mathbf{C} & \dots \\ \frac{\sum_i B_{ri}\Psi_i}{\eta_1} & -\frac{B_{r1}\Psi_1}{\eta_1} \mathbf{C} & [0] & \dots & [0] & \dots \\ [0] & \frac{\sum_i (B_{ri}\Psi_i) - B_{r1}\Psi_1}{\eta_2} & -\frac{B_{r2}\Psi_2}{\eta_2} \mathbf{C} & \dots & [0] & \dots \\ \vdots & \vdots & \vdots & \ddots & [0] & \dots \\ [0] & [0] & [0] & \frac{\sum_{i=1}^n (B_{ri}\Psi_i) - \sum_{i=1}^m B_{ri}\Psi_i}{\eta_m} & -\frac{B_{rm}\Psi_m}{\eta_m} \mathbf{C} & [0] \\ \vdots & \vdots & \vdots & \vdots & \vdots & \ddots \end{bmatrix}. \quad (\text{A7})$$

As before, the portion of material removed from each layer will be resupplied in order to maintain mass balance. The matrix  $\mathbf{C}$  determines the size selectivity of the bioturbation process in the same way as equation (A5). The general equation is provided in equation (A7). The layers transfer a portion (which depends on the bioturbation rate for layer  $i$ ,  $B_{ri}$ , and its depth dependency,  $\Psi$ ) of their smaller than 2 mm classes to the surface layer ( $l_s$ ).

[66] The resupply mechanism is more complex in this case. The surface layer is receiving material from the underlying layers which differ in their contribution (as a function of their depth). This added mass to the surface is balanced by transferring the same amount of mass from the surface layer (but with the full grading spectrum) to the layer below it ( $l_1$ ). This portion of mass is calculated by summing the portion of all contributing layers ( $\sum_i^{LM} B_r \Psi_i$ ; where the

summation is over  $LM$  is the number of contributing layers). This layer is then balanced by transferring the  $\sum_{i=1}^{LM}$  portion to the layer below it and so forth until we reach the bottom of the contributing layers. The layers below the bioturbation domain are unaffected by this process.

[67] **Acknowledgments.** We acknowledge the financial support of Australian Research Council (ARC) grants DP0667093 and DP0556941. S.C. was partially supported by a University of Newcastle Faculty of Science Ph.D. scholarship, and G.R.W. was supported by an ARC Australian Professorial Fellowship. We acknowledge the excellent comments of the reviewers and particularly the insights of Associate Editor Simon Mudd.

## References

- Ahnert, F. (1977), Some comments on the quantitative formulation of geomorphological process in a theoretical model, *Earth Surf. Processes*, 2, 191–201, doi:10.1002/esp.3290020211.
- Burke, B., A. M. Heimsath, and A. F. White (2007), Coupling chemical weathering with soil production across soil mantled landscapes, *Earth Surf. Proc. Landforms*, 32, 853–873, doi:10.1002/esp.1443.
- Cohen, S., G. Willgoose, and G. Hancock (2009), The mARM spatially distributed soil evolution model: A computationally efficient modeling framework and analysis of hillslope soil surface organization, *J. Geophys. Res.*, 114, F03001, doi:10.1029/2008JF001214.
- Gilbert, G. K. (1877), *Report of the Henry Mountains (Utah): U.S. Geological and Geological Survey of Rocky Mountains Region*, 169 pp., U.S. Gov. Print. Off., Washington, D.C.

- Heimsath, A. M., W. E. Dietrich, K. Nishiizumi, and R. C. Finkel (1997), The soil production function and landscape equilibrium, *Nature*, 388(6640), 358–361, doi:10.1038/41056.
- Jenny, H. (1941), *Factors of Soil Formation*, 281 pp., McGraw-Hill, New York.
- Legros, J. P., and G. Pedro (1985), The causes of particle-size distribution in soil profiles derived from crystalline rock, France, *Geoderma*, 36, 15–25, doi:10.1016/0016-7061(85)90060-6.
- Minasny, B., and A. B. McBratney (1999), A rudimentary mechanistic model for soil production and landscape development, *Geoderma*, 90, 3–21, doi:10.1016/S0016-7061(98)00115-3.
- Minasny, B., and A. B. McBratney (2006), Mechanistic soil-landscape modelling as an approach to developing pedogenesis classifications, *Geoderma*, 133, 138–149, doi:10.1016/j.geoderma.2006.03.042.
- Minasny, B., A. B. McBratney, and S. Salvador-Blanes (2008), Quantitative models for pedogenesis: A review, *Geoderma*, 144, 140–157, doi:10.1016/j.geoderma.2007.12.013.
- Ollier, C., and C. Pain (1996), *Regolith, Soil and Landforms*, John Wiley, Chichester, U.K.
- Paton, T. R., G. S. Humphreys, and P. B. Mitchell (1995), *Soils: A New Global View*, 212 pp., Yale Univ. Press, New Haven, Conn.

- Salvador-Blanes, S., B. Minasny, and A. B. McBratney (2007), Modelling long-term in situ soil profile evolution: Application to the genesis of soil profiles containing stone layers, *Eur. J. Soil Sci.*, *58*, 1535–1548, doi:10.1111/j.1365-2389.2007.00961.x.
- Samouëlian, A., and S. Cornu (2008), Modelling the formation and evolution of soils, toward an initial synthesis, *Geoderma*, *145*, 401–409, doi:10.1016/j.geoderma.2008.01.016.
- Sharmeen, S., and G. R. Willgoose (2006), The interaction between armouring and particle weathering for eroding landscapes, *Earth Surf. Proc. Landforms*, *31*, 1195–1210, doi:10.1002/esp.1397.
- Wells, T., P. Binning, and G. R. Willgoose (2005), The role of moisture cycling in the weathering of a quartz chlorite schist in a tropical environment: Findings of a laboratory simulation, *Earth Surf. Processes Landforms*, *30*, 413–428, doi:10.1002/esp.1149.
- Wells, T., P. Binning, G. R. Willgoose, and G. R. Hancock (2006), Laboratory simulation of the salt weathering of schist: I. Weathering of schist blocks in a seasonally wet tropical environment, *Earth Surf. Processes Landforms*, *31*, 339–354, doi:10.1002/esp.1248.
- Wells, T., G. Willgoose, and G. Hancock (2008), Modeling weathering pathways and processes of the fragmentation of salt weathered quartz-chlorite schist, *J. Geophys. Res.*, *113*, F01014, doi:10.1029/2006JF000714.
- White, A. F., and S. L. Brantley (2003), The effect of time on the weathering of silicate minerals: Why do weathering rates differ in the laboratory and field?, *Chem. Geol.*, *202*(3–4), 479–506, doi:10.1016/j.chemgeo.2003.03.001.
- Willgoose, G. R., and S. Riley (1998), The long-term stability of engineered landforms of the Ranger Uranium Mine, Northern Territory, Australia: Application of a catchment evolution model, *Earth Surf. Processes Landforms*, *23*, 237–259, doi:10.1002/(SICI)1096-9837(199803)23:3<237::AID-ESP846>3.0.CO;2-X.
- Willgoose, G. R., and S. Sharmeen (2006), A one-dimensional model for simulating armouring and erosion on hillslopes: I. Model development and event-scale dynamics, *Earth Surf. Processes Landforms*, *31*, 970–991, doi:10.1002/esp.1398.
- Yoo, K., and S. M. Mudd (2008a), Toward process-based modeling of geochemical soil formation across diverse landforms: A new mathematical framework, *Geoderma*, *146*, 248–260, doi:10.1016/j.geoderma.2008.05.029.
- Yoo, K., and S. M. Mudd (2008b), Discrepancy between mineral residence time and soil age: Implications for the interpretation of chemical weathering rates, *Geology*, *36*(1), 35–38, doi:10.1130/G24285A.1.

---

S. Cohen and G. Willgoose, School of Engineering, University of Newcastle, University Dr., Callaghan, NSW 2308, Australia. (garry.willgoose@newcastle.edu.au)

G. Hancock, School of Environmental and Life Sciences, University of Newcastle, University Dr., Callaghan, NSW 2308, Australia.